emergence of a nebular spectrum like those of R Aqr and other fully-fledged members of the class of symbiotic stars. □

Received 5 November 1990; accepted 6 February 1991

1. Merrill, P. W. & Burwell, C. G. *Astrophys. J.* **98,** 153–184 (1943).
2. Bond, H. E., Pier, J., Pilachowski, C., Solvak, M. & Szkody, P. *Bull. Am. Astr. Soc.* **16,** 516 (1984).
3. Tomov, T. *et al. Nature* **346,** 637–638 (1990).
4. Sanduleak, N. & Stephenson, C. B. *Astrophys. J.* **185,** 899–913 (1973).
5. Michalitsianos, A. G. *et al. Astrophys. J.* (in the press).
6. Bode, M. F. & Evans, A. in *Classical Novae* (eds Bode, M. F. & Evans, A.) 163–186 (Wiley, New York, 1989).
7. Stryker, L. L. *et al.* in *A Decade of UV Astronomy with the IUE Satellite* Vol. 1 (ed. Rolfe, E. J.) 149–152 (European Space Agency, Paris, 1988).
8. McNaught, R. H. *et al. IAU Circ.* No. 3969 (1984).
9. Kosai, H., Honda, M. & Wakuda, W. & Norimoto, Y. *IAU Circ.* No. 4281 (1986).
10. Kriscіunas, K. *et al. IAU Circ.* No. 4282 (1986).
11. Wehrse, R., Hauschildt, P. H., Shaviv, G. & Starrfield, S. in *Evolution in Astrophysics* (ed. Rolfe, E. J.) 461–466 (European Space Agency, Paris, 1990).
12. Margon, B. *Nature* **346,** 611 (1990).
13. Michalitsianos, A. G. & Kafatos, M. in *The Symbiotic Phenomenon* (eds Mikolajewska, J., Friedjung, M., Kenyon, S. J. & Viotti, R.) 235–243 (Kluwer, Dordrecht, 1988).

ACKNOWLEDGEMENTS. We thank Y. Kondo for time on the IUE satellite and the IUE observatory staff for their support. S.P.M thanks C. B. Stephenson and J. W. Truran for helpful discussions and acknowledeges a letter from the late N. Sanduleak on the spectral classification of MWC560.

New measurement of the rate coefficient for the reaction of OH with methane

Ghanshyam. L. Vaghjiani* & A. R. Ravishankara†

Aeronomy Laboratory, National Oceanic and Atmospheric Administration, 325 Broadway, Boulder, Colorado 80303 and Cooperative Institute for Research in Environmental Sciences, University of Colorado, Boulder, Colorado 80309, USA

METHANE is an important greenhouse gas, whose concentration in the troposphere is steadily increasing. To estimate the flux of methane into the atmosphere and its atmospheric lifetime, its rate of removal needs to be accurately determined. The main loss process for atmospheric methane is the reaction with the hydroxyl radical OH. We have measured the rate coefficient for this reaction in carefully controlled experiments and found it to be smaller than currently accepted values. Our results indicate a longer CH_4 lifetime (by ~25%) and a correspondingly smaller flux (by ~100 Tg CH_4 yr^{-1}) than previously calculated.

Of all the trace tropospheric species (that is, excluding H_2O and CO_2) methane contributes most to the infrared heating of the atmosphere[1,2]. Methane is also the most abundant hydrocarbon in the troposphere where it modulates the concentration of the OH free radical and serves as a source of CO. Transport of methane to the stratosphere provides a termination step, via the $Cl+CH_4$ reaction, for the chlorine-catalysed destruction of ozone. The oxidation of methane in the stratosphere is an important source of water vapour in this region. During the past decade[3–5] the abundance of methane in the troposphere has been increasing at a rate between 16 and 13 parts per 10^9 volume (p.p.b.v.) per year. The total input and the identities and strengths of the different atmospheric methane sources are not clearly defined. To understand the atmospheric effects of methane, and possibly to regulate it, we need these parameters. At present, the total flux of methane into the atmosphere is estimated from the measured steady-state abundance and the known removal rate of methane[6]. It has been generally accepted that the only process by which methane is chemically degraded in the troposphere is the reaction with OH. Therefore, the rate coefficient, k_1, for the reaction

$$OH + CH_4 \rightarrow CH_3 + H_2O \qquad (1)$$

is important in estimating the total flux of methane. The other loss processes, which are expected to be minor pathways, are surface deposition and reaction with Cl atoms in the lower stratosphere and upper troposphere.

A close examination of the available data[7] shows that only in three investigations[8–10] was k_1 measured below 298 K, the temperature region most important to the atmosphere. Only Davis *et al.*[8] measured k_1 down to 240 K. Reaction 1 is slow. Therefore, at low temperatures, the presence of reactive impurities and occurrence of secondary reactions in laboratory systems can result in an overestimate of k_1. We studied reaction 1 using an experimental method in which secondary chemistry could be minimized and the systematic errors reduced.

The pulsed photolysis-laser induced fluorescence (PP-LIF) method,[11] which is widely used for measuring free radical reaction rate coefficients, was employed here. The specific apparatus employed for the present study, the procedures for measuring OH reaction rate coefficients and the data analysis scheme are described elsewhere[12]. The PP-LIF method relies on measuring the relative rate of change with time of the OH concentration, following its instantaneous production, in the presence of a known excess of methane. The bimolecular rate coefficient, k_1, is obtained by measuring the first-order rate coefficient for the loss of OH, k', in various concentrations of methane. The main

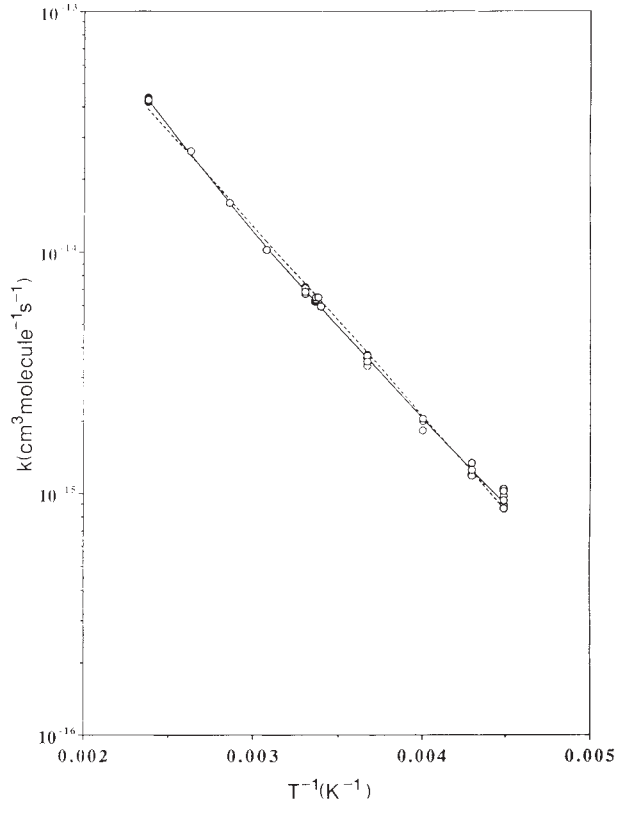

FIG. 1 Plot of k_1 (on a logarithmic scale) against T^{-1}. The 2σ precision of each point is less than its width on the graph. The data adequately fit the expression $k_1 = (2.94 \pm 0.34) \times 10^{-12} \exp[-(1815 \pm 30)/T]$ cm^3 molecule^{-1} s^{-1} (equation 2, dashed line). Errors are 2σ and refer to precision only. The plot is slightly curved and a better fit is given by the expression $k_1 = 1.59 \times 10^{-20} T^{2.84} \exp(-978/T)$ cm^3 molecule^{-1} s^{-1} (equation 3, solid line). We believe from the IR analysis of our sample that the curvature is not due to impurities. Such curvature has been seen in many other systems when k_1 has been measured over a large temperature range.

* Present address: University of Dayton Research Institute, Air Force Astronautics Laboratory, AL/LSCC, Edwards AFB, California 93523, USA.
† Address correspondence to this author at NOAA. Also affiliated with: Department of Chemistry and Biochemistry, University of Colorado, Boulder, Colorado, USA.

TABLE 1 Experimental conditions and measured value of k_1

Temperature (K)	$[OH]_0$ (10^{10} cm^{-3})	[Photolyte]*	Range of $[CH_4]$ (10^{16} cm^{-3})	k_1 (10^{-15} cm^3 molecule^{-1} s^{-1})§	Temperature (K)	$[OH]_0$ (10^{10} cm^{-3})	[Photolyte]*	Range of $[CH_4]$ (10^{16} cm^{-3})	k_1 (10^{-15} cm^3 molecule^{-1} s^{-1})§
420	3.3	1.1	0.6–6.6	43.04 ± 0.47	273	15.3	5.1	10.3–60.1	3.64 ± 0.05
420	1.1	1.1	0.7–4.3	41.84 ± 0.61	273	188.0	15.7‡	9.9–41.3	3.67 ± 0.04
420	3.4	3.4	0.7–4.1	43.66 ± 0.56	273	100.0	9.0‡	10.2–67.0	3.75 ± 0.05
420	10.1	3.4	0.8–6.6	43.36 ± 0.63	273	45.0	19.4, 1.7†	13.8–55.2	3.71 ± 0.16
420	3.3	1.1	1.5–8.9	42.44 ± 0.57	273	45.0	47.1, 1.7†	20.4–79.7	3.38 ± 0.07
420	3.6	1.2	0.9–8.0	42.53 ± 0.52	273	14.1	4.7	13.1–33.9	3.52 ± 0.07
420	3.6	1.2	1.9–8.2	42.87 ± 0.52	273	15.3	5.1	5.5–32.5	3.50 ± 0.05
380	3.3	1.1	0.6–5.6	26.17 ± 0.42	250	15.3	5.1	14.2–98.9	1.98 ± 0.03
					250	14.7	4.9	6.0–45.7	2.04 ± 0.05
350	3.3	1.1	1.1–7.7	15.98 ± 0.11	250	14.4	4.8	8.7–28.0	1.82 ± 0.02
325	3.3	1.1	1.1–5.4	10.26 ± 0.15	233	9.9	3.3	14.3–70.1	1.21 ± 0.02
					233	3.3	1.1	13.7–73.2	1.19 ± 0.01
303	15.0	5.0	10.4–32.1	7.12 ± 0.38	233	1.1	1.1	7.8–36.4	1.18 ± 0.03
303	44.1	14.7	8.0–38.4	7.15 ± 0.11	233	10.2	3.4	10.1–63.3	1.18 ± 0.02
303	15.0	15.1	7.8–39.4	6.74 ± 0.08	233	9.6	3.2	9.9–61.1	1.25 ± 0.03
303	5.1	5.1	7.3–34.4	6.74 ± 0.13	233	9.9	3.3	12.6–72.9	1.33 ± 0.02
303	15.3	5.1	13.3–58.2	7.13 ± 0.18	233	47.0	4.2‡	10.8–72.8	1.25 ± 0.02
303	90.0	3.0†	18.7–74.1	6.84 ± 0.25					
					223	3.0	1.0	8.5–48.3	0.86 ± 0.02
298	15.3	5.1	15.1–71.5	6.20 ± 0.18	223	25.0	2.5‡	9.8–49.8	1.03 ± 0.02
298	15.0	5.1	7.2–48.9	6.30 ± 0.07	223	3.0	1.0	9.1–30.0	0.88 ± 0.04
					223	0.9	0.3	5.4–17.1	0.89 ± 0.04
297	28.0	2.3	15.6–442	6.36 ± 0.22	223	5.1	1.0	4.9–26.5	0.86 ± 0.04
297	29.0	2.4	15.1–46.9	6.47 ± 0.06	223	14.8	6.5‡	6.9–40.7	0.89 ± 0.03
					223	14.6	6.2‡	8.4–53.3	0.86 ± 0.02
295	4.8	4.8‡	17.4–44.6	5.92 ± 0.18	223	15.9	3.1‡	9.6–63.5	0.97 ± 0.03
					223	16.3	6.8‡	12.5–63.2	1.04 ± 0.02
					223	14.9	4.9‡	7.6–38.5	1.02 ± 0.02
					223	3.0	1.0	7.0–29.2	0.93 ± 0.03

* Unless otherwise marked, photolyte is H_2O and units are 10^{15} cm^{-3}.

† Photolyte O_3, units 10^{13} cm^{-3}. The $O(^1D)$ was the source of OH. Concentration of OH is approximate. H_2O concentration was varied between 0 and 5) $\times 10^{16}$ cm^{-3}.

‡ Photolyte H_2O_2, units 10^{13} cm^{-3}.

§ Errors are 2σ.

Production of OH used one of three methods: (1) Broad band photolysis of H_2O between 165 nm (quartz cut-off) and 185 nm (water cut-off). Flash lamp energy 0.8–2.5 J; $[OH]_0 \approx 1$–20×10^{10} cm^{-3}; $[H_2O] \approx 1$–50×10^{15} cm^{-3}. Photolysis at $\lambda > 120$ nm (MgF_2 cut-off) was occasionally employed to check for photolysis of CH_4. Different focal length lenses were used to vary the fluence. (2) 248 nm KrF laser photolysis of H_2O_2. This method was used mostly to create very large concentrations of OH. Laser energies ~2–50 mJ cm^{-2} pulse^{-1}; $[OH]_0 \approx 1$–20×10^{11} cm^{-3}; $[H_2O_2] \approx 2$–16×10^{13} cm^{-3}. (3) 248 nm KrF laser photolysis of O_3 followed by reaction of $O(^1D)$ with water or CH_4. This was used to test alternative methods for production of OH where CH_3 radicals are produced. Laser energy ~2 mJ cm^{-2} pulse^{-1}; $[OH]_0 \approx 5$–10×10^{11} cm^{-3}; $[O_3] \approx 2 \times 10^{13}$ cm^{-3}. OH detection was by pulsed-laser-induced fluorescence in the A ← X system. The excitation wavelength was 281.1 nm ($A\,^2\Sigma$, $v'=1 \leftarrow X\,^2\Pi$, $v''=0$). Fluorescence was monitored at 312.2 ($A^2\Sigma$, $v'=1 \rightarrow X^2\Pi$, $v''=0$) and 306.4 nm ($A^2\Sigma$, $v'=1 \rightarrow X^2\Pi$, $v''=0$). Detection sensitivity was $\sim 1 \times 10^7$ cm^{-3} for 100 laser shots in the absence of CH_4. The buffer gas was helium or nitrogen (100–300 torr). Gas flow rates were 2–8 cm s^{-1} through the reactor. Essentially all reactants are replaced between consecutive photolysis pulses (0.1 s apart at the higher flow rate).

OH removal process is reaction 1; minor contributions come from diffusional loss from the detection zone and reaction with bath gas impurities. The first-order rate coefficient for the latter two processes, k_d, is determined by measuring the OH loss rate in the absence of methane. We determine the concentration of methane by measuring the mass flow rates of methane, the diluent gas and the photolyte/diluent mixture (using calibrated electronic mass flow meters) and by measuring the total pressure (using a capacitance manometer). We can thus determine methane concentrations, and hence k_1, very accurately ($2\sigma \leqslant 5\%$).

Table 1 describes the experimental conditions employed to measure k_1. Fifty measurements of k_1, between 223 and 420 K, are listed in Table 1. Variation of $[OH]_0$, due to variations in photolysis fluence and the concentration of the photolyte, did not affect the measured values of k_1. The variations in photolysis fluence, flow rate of the gases, pressure and the nature of the diluent are not explicitly shown in the table. These variations also did not alter the measured values of k_1. This demonstrates the absence of significant errors due to secondary reactions in our measurements, a point which will be discussed further. Our sample of methane was better than 99.99% pure. The levels of reactive impurities, propene and ethene, were found from infrared measurement to be less than 0.2 p.p.m.v. and 0.7 p.p.m.v. respectively. Thus they contributed less than 2% to the measured value of k_1 even at 223 K, the lowest temperature of our study. The measured values of k_1, and the fit of the data, are shown in Fig. 1. In one set of experiments (not shown in Table 1) we used a discharge-flow laser magnetic resonance system at 296 K to check the results from the pulsed photolysis experiments. The measured value of k_1 was 6.5×10^{-15} cm^3 molecule^{-1} s^{-1}, in excellent agreement with the flash photolysis results.

Our values of k_1 are smaller than those obtained earlier. The difference is close to the estimated uncertainties of the previous measurements and may not be considered significant. However, because of its significance to atmospheric chemistry, this difference is important. We believe that the principal reason for the smaller values measured here is that we have minimized the secondary reactions, especially the reaction of OH with the CH_3 product. To assess their contributions to the measured values of k_1, we calculated the [OH] temporal profiles expected from the reactions shown in Table 2 by numerical integration. This scheme takes into account all reactions that could affect the measured [OH] temporal profiles. We carried out calculations for the concentrations used by Jeong and Kaufman[10] and Davis

et al.[8] as well as those used here. These two studies were chosen because they are the main sources for the currently recommended values of k_1 at lower atmospheric temperatures, they represent two of the most commonly used methods for measuring radical-molecule reaction rate constants (including k_1) and they report the initial conditions used. The rate coefficients for the loss of CH_3 radicals listed in Table 2 are the best available data for our experimental conditions. They were changed as appropriate to correspond to the conditions of other simulations. The simulations show that the rate coefficients reported earlier[8,10] are overestimated by at least 15% at 273 K because of the contribution of the $OH + CH_3$ reaction. In our experiments, on the other hand, the contributions were less than 2%. If the rate coefficient for the $CH_3 + H$ reaction is taken to be the measured value[13], then the importance of $CH_3 + OH$ reaction (and the associated error) increases in the experiments of Davis *et al.* Similarly, a decrease in the CH_3 wall loss or self-reaction rate would increase the errors of Jeong and Kaufman's experiments. The overestimation depends on the value of the rate coefficient for the $OH + CH_3$ reaction, for which there is only one measurement[14]; if the rate coefficient is smaller than this, the overestimation in earlier papers will be reduced. Without knowing the exact experimental conditions used by previous investigators, it is difficult to estimate the contributions of secondary chemistry. This modelling exercise is just to show that secondary reactions involving CH_3 were significant in most previous measurements. The variation of the measured k_1 with experimental parameters is the best evidence for the secondary reactions. Figure 2 shows the data of Davis *et al.* and indicates

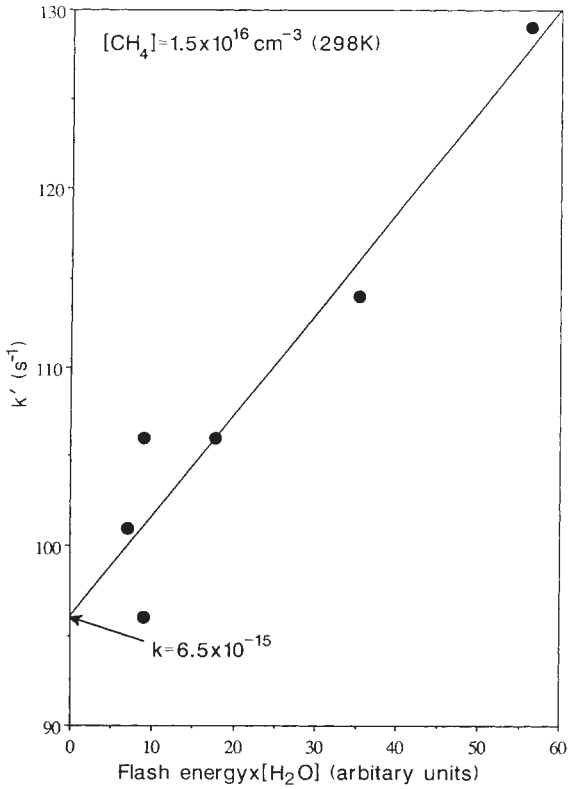

FIG. 2 Plot of the first order rate coefficient k' for the reaction of OH with CH_4 (1.5×10^{16} cm^{-3}) against the product of $[H_2O]$ and flash energy, from the experiments of Davis *et al.*[8] (their table 1). The difference between the first order rate coefficients measured in the presence and absence of CH_4 is k'. The product of the flash energy and $[H_2O]$ is a relative measure of $[OH]_0$, the initial concentration of OH. To keep the photolysis wavelength the same, we have only plotted those results for which a sapphire window was used. The intercept, which is the value of k' in the absence of the $OH + CH_3$ secondary reaction, yields $k_1 = 6.5 \times 10^{-15}$ cm^3 molecule s^{-1}, in good agreement with our value. The slope of the plot is related to the rate of the $OH + CH_3$ reaction, but cannot be evaluated because we do not know the absolute concentrations of OH that were used.

TABLE 2 Kinetic scheme and rate coefficients used in the Runge-Kutte integration of [OH] temporal profiles at 273 K

Reaction	Rate coefficient*, cm^3 molecule^{-1} s^{-1}	Reference
$CH_4 + OH \rightarrow CH_3 + H_2O$	9.0×10^{-16}	
$CH_3 + OH \rightarrow$ Products†	9.0×10^{-11}	14, 15
$CH_3 + H + M \rightarrow CH_4 + M$	2.0×10^{-10}	13
$CH_3 + CH_3 + M \rightarrow C_2H_6 + M$	5.5×10^{-11} to zero‡	17
$CH_3 \rightarrow$ loss	20 (s^{-1})	assumed§
$H \rightarrow$ loss	20 (s^{-1})	assumed§
$H + OH + M \rightarrow H_2O$	4.0×10^{-12}	16, 17
$OH + OH + M \rightarrow H_2O_2$	3.1×10^{-12}	16, 17

* For simulations of experiments carried out in a flow tube[10] at 3 torr, or in flash photolysis apparatus[8] at ~25 torr, the pressure-dependent rate coefficients were changed appropriately. Many of the rate coefficients are set to minimize the effect of secondary reactions in these studies.

† We assume that the product of the $CH_3 + OH$ reaction does not react with OH. If it did, it would lead to further overestimation of k_1.

‡ The rate coefficient for the $CH_3 + CH_3$ reaction depends on pressure and bath gas. If this reaction is fast, it suppresses the $OH + CH_3$ reaction. To simulate our experiments, this value was set to zero to maximize $[CH_3]$, whereas when we simulated the experiments of Jeong and Kaufman and Davis *et al.* it was set to the maximum value to minimize $[CH_3]$.

§ In the experiments involving the flash photolysis of H_2O, $[H]_0$ is assumed to be the same as $[OH]_0$.

that k_1 was indeed overestimated in their experiments. A similar plot of our data at 223 K (the temperature at which the effect would be most evident) yields an intercept which is within one standard deviation of the mean at that temperature. Furthermore, the correlation coefficient, R^2, of our plot is only 0.47. Any contributions from the impurities in the samples used by Jeong and Kaufman[10] and Davis *et al.*[8] would only make k_1 larger.

The chief effect of revising the value of k_1 is to alter the CH_4 budget. All atmospheric processes that are now evaluated from the measured atmospheric CH_4 concentration, such as the current flux of CH_4 to the stratosphere, will be unaffected by the change in k_1. Generally, k_1 values recommended by the NASA[16] or the CODATA[17] panels are used for atmospheric lifetime and budget calculations. A crude way to appraise the atmospheric significance of our results is to examine the values of k_1 at 273 K, the weighted mean temperature at which the removal of a species such as methane, with a lifetime of several years, will take place. The NASA and CODATA values, at 273 K are respectively 24% and 29% higher than those predicted by equation (3) in Fig. 1. Our results indicate that the lifetime of methane in the troposphere is ~25% longer and the flux ~25% (~100 Tg yr^{-1}) smaller than currently accepted values. This change in flux is comparable to or less than every one of the main sources[6,18]. More detailed modelling calculations, which take into account the effects of feedback, use temperature and OH fields and include transport, can better assess the effect of this revision in k_1. Such a calculation by Valentin and Crutzen (personal communication) shows that the methane lifetime is ~20% longer when our values are used instead of the CODATA recommendation. They also show that using our values 490 Tg yr^{-1} of CH_4 is removed through OH reaction, as opposed to 590 Tg yr^{-1} of CH_4 using the CODATA recommendation. Conversely, if the flux of methane into the troposphere is indeed 590 Tg yr^{-1}, then there is a missing sink for CH_4 in the troposphere. □

Received 19 December 1990; accepted 13 February 1991.

1. Ramanathan, V., Cicerone, R. J., Singh, H. B. & Kiehl, J. T. *J. geophys. Res.* **90,** 5547-5566 (1985).
2. Mitchell, J. F. B. *Rev. Geophys.* **27,** 115-139 (1989).
3. Steele, L. P. *et al. J. atmos. Chem.* **5,** 125-171 (1987).
4. Khalil, M. A. K. & Rasmussen, R. A. *Envir. Sci. Technol.* **24,** 549-553 (1990).
5. Blake, D. R. & Rowland, F. S. *Science* **239,** 1129-1131 (1988).
6. Cicerone, R. J. & Oremland, R. S. *Global biogeochem. Cycles* **2,** 299-327 (1988).
7. Ravishankara, A. R. *Ann. Rev. phys. Chem.* **39,** 367-394 (1988).

8. Davis, D. D., Fischer, S. & Schiff, R. *J. chem. Phys.* **61,** 2213–2219 (1974).
9. Margitan, J. J., Kaufman, F. & Anderson, J. G. *Geophys. Res. Lett.* **1,** 80–81 (1974).
10. Jeong, K. M. & Kaufman, F. *J. phys. Chem.* **86,** 1808–1815 (1982).
11. Hancock, G. *Measurements of Thermal Rate Data* in *Modern Gas Kinetics: Theory, Experiment and Applications* (eds Pilling, M. J. & Smith, I. W. M., Blackwell, Oxford, 1987).
12. Vaghjiani, G. L. & Ravishankara, A. R. *J. phys. Chem.* **93,** 1948–1959 (1989).
13. Brouard, M., McPherson, M. T. & Pilling, M. J. *J. phys. Chem.* **93,** 4047–4059 (1989).
14. Sworski, T. J. & Hochanadel, C. J. & Ogren, P. J. *J. phys. Chem.* **84,** 129–134 (1980).
15. Tsang, W. & Hampson, R. F. *J. phys. chem. Ref. Data* **15,** 1087–1279 (1986).
16. DeMore, W. B. *et al. NASA JPL Publ.* 90-1 1990.
17. Atkinson, R. *et al. J. phys. chem. Ref. Data* **18,** 881–1097 (1989).
18. Taylor, J. A., Brasseur, G., Zimmerman, P. & Cicerone, R. J. *J. geophys. Res.* **96,** 3013–3044 (1991).

ACKNOWLEDGEMENTS. We thank K. Valentin and P. Crutzen for helpful discussions and calculations; R. J. Cicerone for valuable discussions and the pre-print of his paper; D. Bopegedera and J. B. Burkholder for analysis of our methane samples; T. Gierczak and R. Talukdar for the flow tube measurements; and C. J. Howard and D. L. Albritton for reading the manuscript. This research was carried out under the Radiatively Important Trace Species component of the NOAA Climate and Global Change Program.

Effects of ice coverage and ice-rafted material on sedimentation in the Fram Strait

Dierk Hebbeln & Gerold Wefer

Universität Bremen, Geowissenschaften, Postfach 330440, 2800 Bremen 33, FRG

As little is known about pelagic sedimentation processes in Arctic environments[1], the interpretation of biological and chemical processes, as well as the reconstruction of ancient conditions, including those in the glacial North Atlantic, is difficult. Here we provide sediment-trap results, which show that the position of the sea-ice boundary significantly influences the particle flux. The seasonal variability of the particle flux differed markedly in the various sediment-trap sites in Fram Strait, depending on the behaviour of the sea ice. Under complete ice cover, sedimentation is very low, whereas maximum sedimentation is found at the ice margin. The highest particle flux observed, showing a large lithogenic component, was observed at the ice edge where the water was warmer (>2 °C). We find that high biogenic opal fluxes are characteristic of the summer ice margin, indicating that the sedimentary record of opal fluxes may allow the position of ice margins in the past to be reconstructed.

In the Fram Strait, the narrow gateway between the North Atlantic and the Arctic Ocean, areas with constant and seasonal ice coverage, as well as ice-free areas are present (Fig. 1). The large variability in seasonal ice coverage is caused by a complex system of warm (West Spitsbergen) and cold (East Greenland) currents (Fig. 1). As there is such a large spatial and seasonal variability in ice cover, the Fram Strait is particularly well suited for the study of the relation between ice coverage and particle sedimentation.

Three one-year trap deployments were positioned east–west across the Fram Strait (Fig. 1) site FS4 was permanently ice-covered, whereas another (FS3) was ice-covered for about six months. The third site (SP2) was located at the winter ice margin, close to the Spitsbergen shelf edge. The 20-cup-collector sediment traps, with a collection area of 0.5 m^2, were attached to moored arrays at depths ranging from 1,110 to 1,488 m. Depending on the expected ice cover, samples were taken at intervals of between 11.5 and 23 days. Field work and laboratory analyses are described elsewhere[2]. The flux rates of individual components are given in Fig. 2.

Site FS4 was located in the East Greenland Current, which is characterized by year-round water temperature <0 °C. The annual particle flux is 2.9 g m^{-2} (Fig. 2*a*), and was the lowest of the three sites, with a maximum from August to October and a minimum between January and April. Site FS3 was in the Central Fram Strait in an area where the ice margin fluctuates for 70% of the year[3]. During this time, the water temperature is near 0 °C. The annual particle flux was 60.5 g m^{-2} (Fig. 2*b*), with the daily flux ranging from a maximum of 700 mg m^{-2} d^{-1} in July, to between 11 and 21 mg m^{-2} d^{-1} for December and January. The eastern part of the Fram Strait is ice-free most of the year, but during 1989, pack ice reached site SP2 in January. Because the water temperature of the West Spitsbergen Current is higher than 0 °C, the ice melts rather quickly. The total annual flux at this site was 149.9 g m^{-2} (Fig. 2*c*), and was the highest measured at the three sites. The seasonal variation in the flux differed from those observed further west in the time at which the flux increased. Between July and December, a more or less continuous flux of 80 to 210 mg m^{-2} d^{-1} was measured. In January the total flux then increased, reaching 1,147 mg m^{-2} d^{-1}, followed by a decrease reaching ~500 mg m^{-2} d^{-1} in May. A change in the flux composition was also observed; from July to December the particle flux was dominated by fecal pellets, whereas from January to April quartz grains of silt- to fine sand-size were common.

The most important factors influencing sedimentation are therefore the presence of ice and the surface water temperatures.

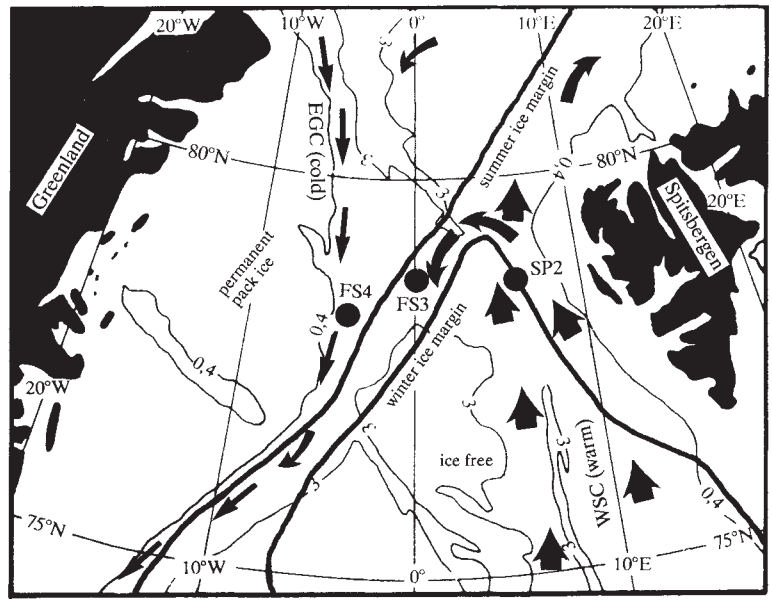

FIG. 1 Positions of trap sites FS4 (78° 26.5′ N, 04° 05.7′ W, water depth 1,763 m, trap depth 1,191 m), FS3 (78° 45.8′ N, 00° 10.7′ E, water depth 2,487 m, trap depth 1,488 m) and SP2 (78° 53.4′ N, 06° 44.5′ E, water depth 1,661 m, trap depth 1,110 m) in the Fram Strait. The average position of ice margins[13] and the cold East Greenland Current (ECG) and the warm West Spitsbergen Current (WSC) are also shown.